PHYSICAL REVIEW B **83**, 205129 (2011)

Ab initio electronic structure of thallium-based topological insulators

S. V. Eremeev,[1,2,3] G. Bihlmayer,[4] M. Vergniory,[3] Yu. M. Koroteev,[1] T. V. Menshchikova,[2] J. Henk,[5] A. Ernst,[5] and E. V. Chulkov[3,6,*]

[1]*Institute of Strength Physics and Materials Science, pr. Academicheskii 2/4, 634021, Tomsk, Russia*
[2]*Tomsk State University, pr. Lenina 36, 634050, Tomsk, Russia*
[3]*Donostia International Physics Center (DIPC), Paseo Manuel de Lardizabal 4, ES-20018 San Sebastián/Donostia, Basque Country, Spain*
[4]*Institut für Festkörperforschung and Institute for Advanced Simulation, Forschungszentrum Jülich and JARA, DE-52425 Jülich, Germany*
[5]*Max-Planck-Institut für Mikrostrukturphysik, Weinberg 2, DE-06120, Halle, Germany*
[6]*Departamento de Física de Materiales, Centro de Física de Materiales CFM - MPC and Centro Mixto CSIC-UPV/EHU, Facultad de Ciencias Químicas, Universidad del Pais Vasco/Euskal Herriko Unibertsitatea, Apdo. 1072, 20080 San Sebastián/Donostia, Basque Country, Spain*

(Received 4 December 2010; revised manuscript received 24 February 2011; published 25 May 2011)

We analyze the crystal and electronic structures of Tl-based strong topological insulators $TlSbTe_2$, $TlSbSe_2$, $TlBiTe_2$, and $TlBiSe_2$ by using first-principles calculation results. The topological nature of these materials is characterized by a single Dirac cone at the $\overline{\Gamma}$ point. Aside from the latter robust surface state (SS), we find trivial SSs at (around) the Fermi level for large momenta as well as deep trivial SSs at (around) $\overline{\Gamma}$. The calculated energy cuts show an isotropic shape of the Dirac cone and a simple spin structure of the cone. The strong dependence of electronic structure on both optimization of the chalcogenide atom position in bulk and surface relaxations, as well as the slow convergence of the Dirac cone with respect to the film thickness, are discussed. The situation in the thallides is contrasted with results for isostructural indium compounds $InBiTe_2$ and $InSbTe_2$, the latter not being topological insulators.

DOI: 10.1103/PhysRevB.83.205129 PACS number(s): 73.20.−r, 79.60.−i

I. INTRODUCTION

Three-dimensional topological insulators are narrow-gap semiconductors that are characterized by an inverted energy gap at some symmetry points of the bulk Brillouin zone (BZ) due to strong spin-orbit interaction.[1–3] An important consequence of the topological nature of these semiconductors is a surface state (SS) that makes the semiconductor surface conducting.[1–4] This surface state shows linear dispersion, forming a Dirac cone with a crossing (Dirac) point at (around) the Fermi level (E_F).[1–4] In contrast to the Dirac cone in graphene, this topological SS, being spin-orbit split, carries only a single electron per momentum with a spin that changes its direction consistently with a change of momentum. The topological origin of the SS protects the Dirac cone from surface perturbations,[1] and even under such a strong perturbation as removing of the surface Te (Se) atomic layer of tellurium (selenium) chalcogenides, this surface state survives.[5] The unique surface properties of topological insulators make these materials important for many potential applications, in particular, in spintronics and quantum computing.

Recently, it was shown both experimentally[6–9] and theoretically[4,5,10–12] that binary layered semiconductor compounds Bi_2Te_3, Bi_2Se_3, and Sb_2Te_3 are three-dimensional (3D) strong topological insulators with the topological SS mostly located in the first five-layer block (quintuple layer) adjacent to the vacuum side.[5,12] Very recently, it was also shown that some layered ternary compounds with tetradymitelike crystal structure such as $PbBi_4Te_7$,[13,14] $PbBi_2Te_4$,[15,16] $SnSb_2Te_4$,[14,15] and others should be topological insulators. Another family of narrow-gap semiconductors, thallium-based chalcogenides of Bi and Sb, with nontetradymitelike crystal structure, have been theoretically predicted to be a new family of 3D topological insulators with a single Dirac cone at the $\overline{\Gamma}$ point.[17–19] Photoemission measurements confirmed that indeed $TlBiSe_2$ (Refs. 20–23) and $TlBiTe_2$ (Ref. 22) are topological insulators showing a clear Dirac-type dispersion of the SS at E_F.

In this paper, we present detailed *ab initio* calculation results for this family of topological insulators, namely, narrow-gap Tl-based ternary compounds $TlBiTe_2$, $TlBiSe_2$, $TlSbTe_2$, and $TlSbSe_2$. In contrast to the aforementioned A_2B_3 compounds, where A is one of Bi or Sb and B can be a chalcogenide such as Te or Se, the $TlAB_2$ compounds are not characterized by a layerlike structure and the three-dimensional bonding leads to distinctly different properties of the surface states arising in these materials. While the surface electronic structure of the layered A_2B_3 semiconductors is quite insensitive to surface structural modifications (relaxations),[5] the surface electronic states of the Tl-based compounds show a remarkable sensitivity to surface relaxations, different terminations, etc. We find that deeply penetrating surface states and the depth of penetration varies with the energy position of these states in the bulk-projected band gap. In the A_2B_3 compounds, the preferred cleavage plane is in-between two weakly (van der Waals) bonded quintuple layers, while in the $TlAB_2$ family, the surface formation leads to breaking of chemical bonds. Consequently, the formation of additional surface states can be expected that complicate the simple "single Dirac-cone picture" found in the systems with van der Waals–bonded layers. Other properties, such as superconductivity,[24] arise in this family of compounds, which makes them potentially interesting to study the interplay with the properties introduced by the topological nontriviality. Recent angle-resolved photoemission studies[20–23] allow a comparison of the calculated surface band structure with experimental results.

To illustrate the complex character of the Tl-based semiconductor surfaces, we also present *ab initio* calculation results for indium-based compounds $InBiTe_2$ and $InSbTe_2$, which crystallize in the $TlBiTe_2$-like crystal structure. In

contrast to the thallides, the In-based compounds are not topological insulators. For example, $InBiTe_2$ shows similar surface electronic states except for the Dirac-cone feature, demonstrating that $InBiTe_2$ is a topologically trivial material.

II. CALCULATION METHODS

The structural optimization and electronic structure calculations were performed within the density-functional formalism implemented in VASP.[25,26] In this plane-wave approach, the interaction between the ion cores and valence electrons was described by the projector augmented-wave method.[27,28] To describe the exchange-correlation energy, we used the generalized gradient approximation (GGA).[29] The Hamiltonian contained the scalar relativistic corrections and the spin-orbit coupling was taken into account by the second variation method.[30] We checked the effect of including d electrons of Tl and Bi(Sb) in valence electrons in bulk calculations and found it negligible in the vicinity of the gap. So, in the presented calculation results, the d electrons were considered as core electrons.

Complementary calculations were performed using the full-potential linearized augmented plane-wave method in thin-film geometry[31,32] as implemented in the FLEUR code.[33] Spin-orbit coupling was included in the self-consistent calculations as described in Ref. 34. The semicore d states of Tl and In were included as local orbitals in the valence window in this case. We compared the results of the structural relaxation for some bulk cases with those obtained from the VASP calculations and found very good agreement between the two sets of data. Therefore, we show all the results obtained with relaxations provided by the latter technique.

The film calculations presented in this work were performed using symmetric setups, so the upper and lower surfaces are identical. In these cases, deviations from the ideal stoichiometry occur, so the position of the Fermi level depends on the termination and film thickness. Therefore, we adjusted the bands of the film calculations to the projected bulk band structure and obtained the Fermi level from the latter to simulate a surface of a semi-infinite crystal.

III. RESULTS AND DISCUSSION

A. Bulk properties

The crystal structure of the thallides, $TlAB_2$, can be viewed as a sequence of hexagonally close-packed layers where the elements follow the order Tl-B-A-B-Tl-B-A-B-. . . (see Fig. 1). The hexagonal unit cell characterized by lattice parameters a and c consists of 12 atomic layers that would be separated by equal distances $c/12$ if the internal parameter u of the B atom is equal to $1/4$. In the case $u < 1/4$, the ideal layer spacing of $c/12$ between the A and B planes is reduced by $c(0.25 - u)$ and enlarged by the same amount between Tl and B. The total-energy-optimized lattice and internal parameters are given in Table I. Our lattice parameters are, on average, 0.9% larger than those given by Hoang and Mahanti,[35] which are close to the experimental values. The internal parameters are not given in Ref. 35. However, we can compare u with experimental data[36] for the tellurides and find a systematically smaller theoretical u by 1.4%. Also, in a recent calculation,[19] a value of $z_{Te} = 0.21$ Å, which

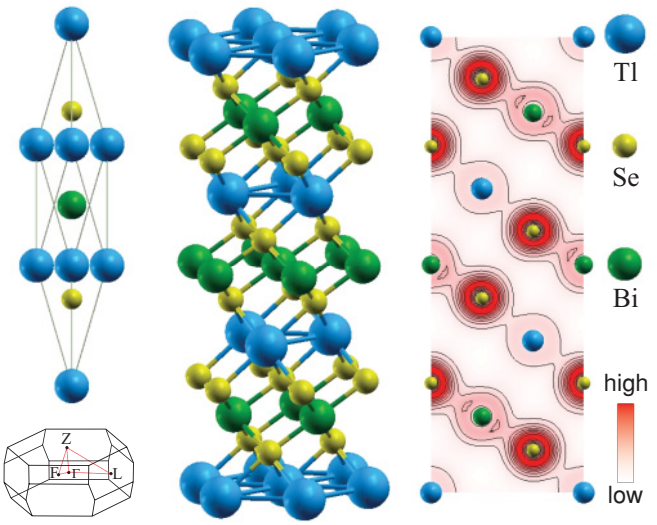

FIG. 1. (Color online) Atomic structure of $TlBiSe_2$ in rhombohedral and hexagonal bases (left), and charge-density distribution in $(11\bar{2}0)$ plane of the hexagonal cell (right). The Brillouin zone for the rhombohedral cell is shown in the lower left corner.

corresponds to $u = 0.241$, was found for $TlSbTe_2$, that is, slightly smaller than the experimental value of $u = 0.243$. In this publication and a recent work,[21] the importance of optimization of the u parameter for the bulk band structure and topological properties was realized.

As it can be seen from the charge density in Fig. 1 (right), the short A-B interlayer distance results from strong covalent bonding between these planes. Although the Tl-B bond is weaker, it is still in the characteristic range of chemical bonding and can not be compared to the van der Waals–bonded quintuple layers of the Bi_2Te_3-type compounds. Nevertheless, it is reasonable to assume a . . .-Tl-B_3-A-B_1, i.e., B_1 termination of the hexagonal (0001) surface.[18] We will use this termination for our calculations, for $TlBiSe_2$; however, we will also compare the calculated surface electronic structure to that for other types of terminations.

The primitive unit cell, which contains only one formula unit, is a rhombohedral one and is characterized by a lattice parameter a_{rh} and an angle α:

$$a_{rh} = \frac{1}{3}\sqrt{3a^2 + c^2}, \quad \cos(\alpha) = 1 - \frac{9}{6 + 2(c/a)^2}. \quad (1)$$

The band structures shown in Fig. 2 are drawn in the reciprocal space of this unit cell. The line $\Gamma - Z$ corresponds to the hexagonal axis and projects electronic bands onto the center

TABLE I. Optimized lattice (a and c) and internal (u) parameters of the selected thallides in hexagonal setup. The distances between the Tl-B and A-B layers can be evaluated as $c(1/3 - u)$ and $c(u - 1/6)$, respectively.

	a (Å)	c (Å)	u
$TlSbTe_2$	4.503	23.624	0.2396
$TlSbSe_2$	4.229	22.598	0.2378
$TlBiTe_2$	4.587	23.665	0.2425
$TlBiSe_2$	4.324	22.537	0.2406

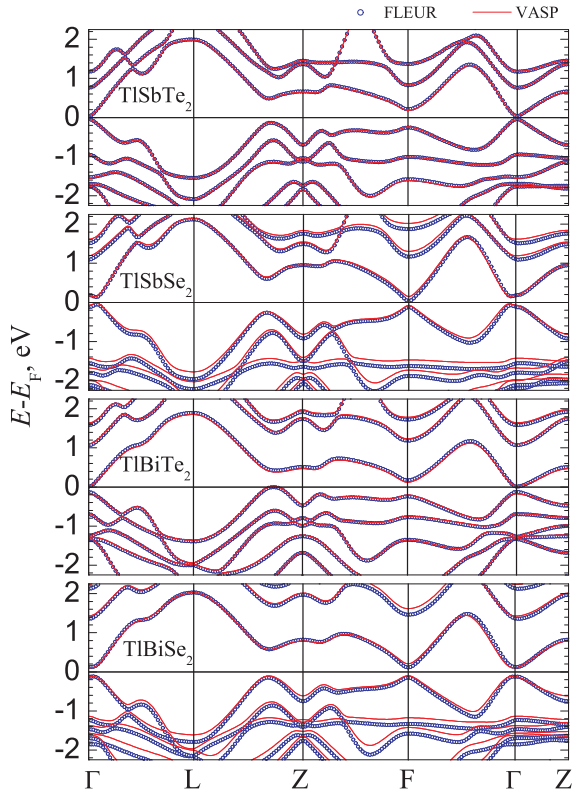

FIG. 2. (Color online) Bulk band structure containing all TRIMs in the Brillouin zone calculated by the VASP (lines) and the FLEUR code (circles). A sketch of the Brillouin zone can be found in Fig. 1. All calculations were performed including spin-orbit coupling.

of the Brillouin zone ($\bar{\Gamma}$ point) of a hexagonal (0001) [rhombohedral (111)] surface. The time-reversal invariant momenta (TRIMs) in this Brillouin zone are the Γ, Z (sometimes called T) points and triply degenerate F and L points. As can be seen from Fig. 2, small direct energy gaps exist at the Γ and F points for all the compounds of interest; therefore, the band inversion due to spin-orbit interaction can be expected at these points only. We checked the parity of the wave functions at all TRIMs to determine the topological character of these bulk materials.[1] In agreement with previous calculations,[17,18] where, specifically, the band inversion at Γ was investigated, we confirm that all four compounds are topological insulators.

Comparing the two computational methods, VASP and FLEUR, we find good agreement, especially in the case of the tellurides. The slightly larger deviation of the results for the selenides might be caused by the chosen Se pseudopotential. Comparison to other calculations[17,35] shows good agreement, e.g., the smaller band gaps of the tellurides and the indirect gap of $TlBiTe_2$ are confirmed by our calculations. However, the bulk projection disagrees with that in Ref. 19 in some important detail, which is due to differences in the bulk crystal structure (especially to ideal $u = 1/4$ used in Ref. 19). Again, we notice the strong sensitivity of the electronic structure on structural details in these compounds.

B. Surface properties

1. *Surface relaxation*

As will be shown below, the surface relaxation is very important for a correct description of the surface band structure in these compounds. From Table II, it can be seen that the surface relaxation has an oscillatory character, starting with a contraction of the first interlayer spacing. This is a typical effect resulting from the lower coordination of the surface layer and known from many metallic and semimetallic systems such as Bi.[37] In contrast to metals, in the $TlAB_2$ compounds, the relaxation displacements decay slowly into the bulk, which is closely related to deep penetration of the charge density of the Dirac surface state. In our calculations, the relaxation for the 12 outermost atomic layers is taken into account. The deeper layers were fixed at their bulk positions.

2. *$TlSbTe_2$*

Figures 3(a) and 3(b) show the electronic structure of the Te-terminated 39-layer $TlSbTe_2(0001)$ slab as calculated by both FLEUR (a) and VASP (b). As one can see, at the $\bar{\Gamma}$ point, both methods give surface states at the conduction-band minimum (CBM) and valence-band maximum (VBM), which resemble a Dirac-type crossing at $\bar{\Gamma}$, but a quite big band splitting ($\approx$50–60 meV) is obtained. In addition to this split Dirac state, other spin-split surface states arise, which propagate in the projected bulk gap around the Fermi level and in the symmetry gap at about -0.7 eV at $\bar{\Gamma}$. In the latter case, these states are more localized in vacuum as compared to the states that cross the Fermi level in the vicinity of the zone center.

The splitting of the Dirac state is caused by the interaction between opposite surfaces of the slab due to the finite slab thickness. As one can see in Fig. 3(c), this state penetrates deeply into the bulk and does not completely decay at the center of the 39-ML slab, in contrast to the trivial surface states, which are localized in a few outer atomic layers only. The splitting of the Dirac state can be suppressed by H termination on one of the sides [inset in Fig. 3(a)] as well as by increasing the slab thickness [Fig. 3(d)].

As was mentioned above, the surface relaxation is important to the surface band structure in these materials. As can be

TABLE II. Changes of the interlayer spacings of the (0001) surfaces of $TlAB_2$ compounds with B termination. All values are given in Å with respect to the ideal, bulk values.

Δ_{ij}	$TlSbTe_2$	$TlSbSe_2$	$TlBiTe_2$	$TlBiSe_2$
$Se(Te)_1$-$Sb(Bi)_2$	−0.132	−0.107	−0.156	−0.147
$Sb(Bi)_2$-$Se(Te)_3$	0.147	0.157	0.211	0.202
$Se(Te)_3$-Tl_4	−0.272	−0.230	−0.295	−0.278
Tl_4-$Se(Te)_5$	0.106	0.167	0.181	0.168
$Se(Te)_5$-$Sb(Bi)_6$	−0.044	−0.047	−0.056	−0.062
$Sb(Bi)_6$-$Se(Te)_7$	0.063	0.077	0.087	0.085
$Se(Te)_7$-Tl_8	−0.131	−0.128	−0.134	−0.142
Tl_8-$Se(Te)_9$	0.088	0.081	0.090	0.083
$Se(Te)_9$-$Sb(Bi)_{10}$	−0.018	−0.023	−0.024	−0.029
$Sb(Bi)_{10}$-$Se(Te)_{11}$	0.040	0.038	0.036	0.035
$Se(Te)_{11}$-Tl_{12}	−0.075	−0.063	−0.059	−0.069
Tl_{12}-$Se(Te)_{13}$	0.037	0.035	0.033	0.025

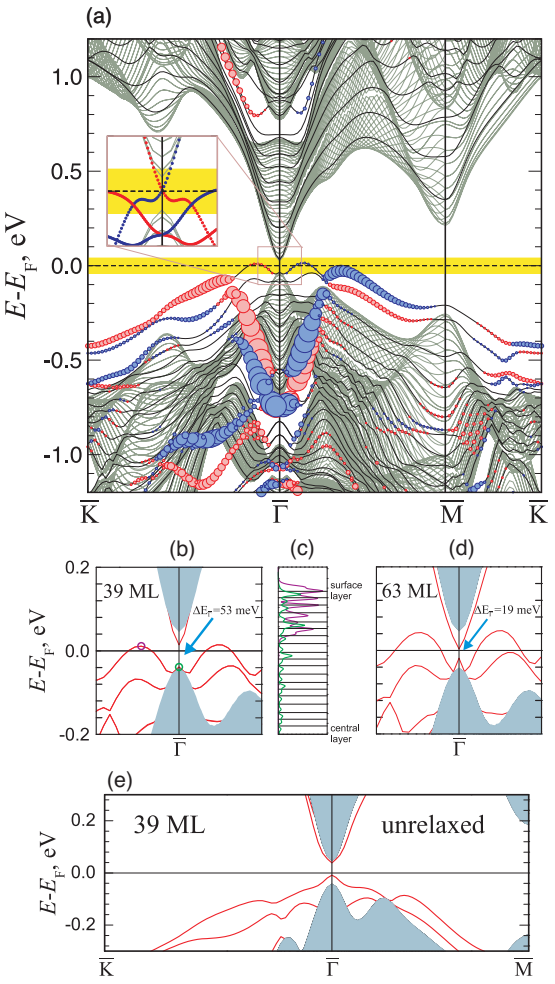

FIG. 3. (Color) (a) Band structure of a symmetric 39-layer $TlSbTe_2$ slab with a Te-terminated (0001) surface (black lines) and the projected bulk band structure (gray) in the background (FLEUR result). The area of the bulk-projected band gap around the $\bar{\Gamma}$ point is indicated with the yellow background. The size of the symbols reflects the weight of the states in the vacuum and the color indicates the spin direction, i.e., parallel or antiparallel to $\mathbf{n} \times \mathbf{k}$, if $\mathbf{n}$ is the surface normal and $\mathbf{k}$ is the wave vector of the state. Inset: Slab with H termination on one of the sides; dotted lines show the state that connects the valence and conduction bands, full lines show a normal, Rashba split surface state. (b) Surface band structure in the vicinity of $\bar{\Gamma}$ for a 39-layer $TlSbTe_2(0001)$ (VASP calculation). Gray areas mark the region of projected bulk states. (c) xy-integrated charge-density distribution for Dirac state (green line) and for trivial surface state (violet line); horizontal lines indicate the atomic-layer positions. (d) Surface band spectrum for a 63-layer $TlSbTe_2(0001)$ slab. (e) Results for an unrelaxed 39-layer film.

realized from the comparison of Figs. 3(d),3(d), and 3(e), which shows the band structure of the unrelaxed surface, in the relaxed case, the upper trivial surface state disperses downward into the bulk valence bands as it approaches the $\bar{\Gamma}$ point. In addition, a Dirac-type state appears from the bulk continuum and disperses upward as it approaches the zone center. These two states are different in localization as can be seen from the size of the symbols in Fig. 3(a) and from charge-density distribution along the z direction shown in Fig. 3(c). In the unrelaxed case, the Dirac state does not split off the bulk edge but appears as a continuation of the trivial state propagating in the bulk gap. The picture similar to our unrelaxed case was also obtained by Lin *et al.* (Fig. 3 in Ref. 19). It should be noted that, for $TlSbTe_2$ as well as for other Tl-based compounds calculated in Refs. 18 and 19 (where the bulk lattice parameters given by Hoang and Mahanti[35]) were used, an almost unsplit Dirac cone was obtained even for slabs of 23-layer thickness. This shows the strong sensitivity of the surface state on the details of the underlying bulk band structure, which is, in the gap region, sensitively dependent on the chosen lattice parameters.

3. $TlSbSe_2$

It is interesting to compare the behavior of the topologically trivial (normal) surface states and the nontrivial Dirac-type state, which connects the valence and conduction bands, in $TlSbTe_2$ with the related $TlSbSe_2$ compound. The bulk band structure (Fig. 2) indicates that the gap around $\bar{\Gamma}$ at the Fermi level is larger in the Se compound, therefore, a more pronounced Dirac-type behavior (smaller splitting, linear dispersion) can be expected. Indeed, we see in Fig. 4 a well-developed surface state in the zone center that shows a smaller splitting than in the $TlSbTe_2$ case. Since the bulk projection in the Se compound is concave at the valence-band maximum and convex at the conduction-band minimum (in the Te compound this is the other way round), a rather wide gap region forms near the $\bar{\Gamma}$ point. The charge density as shown on the right of Fig. 4 decays slightly faster toward the center of the film and the splitting of the states at the zone center is substantially reduced (21 meV for a 39-layer film).

At energies of about -0.9 eV, we see a Rashba-type spin-split surface state in the bulk-projected bulk band gap around $\bar{\Gamma}$ that is strongly localized in the surface region. Entering the region of projected bulk bands, this state quickly loses its surface character. At larger k values, significant surface character appears in the states that cross the band gap as trivial surface states. A significant spin splitting induced by spin-orbit interaction can be observed also in these surface states. In terms of their dispersion and spin splitting, these states

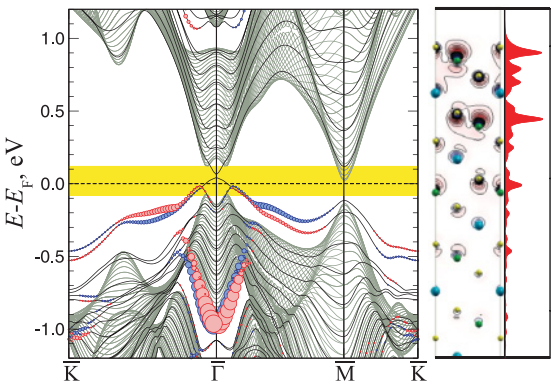

FIG. 4. (Color) Band structure of a symmetric 39-layer $TlSbSe_2$ film with an Se-terminated (0001) surface. The color coding follows the one in Fig. 3. The right panel shows the spatial distribution of the $\bar{\Gamma}$ Dirac-state charge density in the $(11\bar{2}0)$ plane in the upper half of the film and integrated over the (x, y) plane (right).

show similarities to the surface states of semi-infinite Bi(111) and Bi(001) films.[38–40] In the Bi case, this state is only half-occupied, while here we observe full occupation throughout the Brillouin zone. This is not surprising since the surface atom (Se or Te in case of $TlSbTe_2$) has one electron more than Sb that is isoelectronic to Bi. Indeed, we will see below that, in Tl-terminated surfaces, this band is almost unoccupied (Tl has a p^1 configuration, while Sb and Se are p^3 and p^4, respectively).

4. *TlBiTe$_2$*

Recently, surfaces of $TlBiTe_2$ and $TlBiSe_2$ have been studied experimentally with angle-resolved photoemission spectroscopy (ARPES) by Chen e*t al.*[22] In this work, for $TlBiTe_2$, a Dirac-type dispersion was observed at the $\bar{\Gamma}$ point, with a crossing point about -0.3 eV below the Fermi level. One has to note here that E_F depends on the doping of the samples and thus can be varied in some range. The Dirac cone is surrounded by features originating from projected bulk states, which form maxima at -0.2 and -0.3 Å^{-1} in the $\bar{\Gamma}\bar{M}$ and $\bar{\Gamma}\bar{K}$ directions, respectively. Furthermore, we notice that, in the ARPES experiments, no signs of other surface states can be found.[22]

Comparing these findings with our calculation results for the Te-terminated surface [Figs. 5(a) and 5(c)], we observe that the features around the $\bar{\Gamma}$ point are nicely reproduced, except for a small residual splitting of the Dirac state due to the finite film thickness and the fact that, in our calculation, additional surface states are visible in the gap around E_F. From the ARPES data, an intense, V-shaped feature with its minimum in the zone center at -0.7 eV is visible, and it loses intensity at -0.4 eV. In our calculation, this would correspond to the Rashba split surface state in the projected gap at approximately -0.7 eV, which loses surface character when it enters the region of the bulk states.

There are several possible explanations for the absence of the surface states near E_F in the ARPES measurements. For example, depending on the energy or polarization of the light, the photoemission intensity for states with a particular symmetry can be reduced or even suppressed. However, since experimentally no additional surface state is observed either in the $\bar{\Gamma}\bar{M}$ and the $\bar{\Gamma}\bar{K}$ directions, at least a full suppression due to symmetry is unlikely. On the other hand, the surface states could be shifted in energy or completely absent due to the presence of adsorbates or a surface reconstruction. More experimental data would be necessary to check these possibilities. We also note that a different surface termination (with Tl or Bi) could be found experimentally. We will come back to that point in the next section.

In Fig. 5(b), we show the $\bar{\Gamma}$ Dirac-state charge-density distribution in the $(11\bar{2}0)$ plane as well as its charge density as a function of the z coordinate (integrated over the x,y coordinates). One can clearly see that this state decays in the bulk significantly faster compared to that on the $TlSbSe_2$ surface (Fig. 4) and much faster than on $TlSbTe_2$ [Fig. 3(c)]. This closely correlates with the smaller splitting of the Dirac state at $\bar{\Gamma}$.

In Fig. 5(d), constant-energy cuts (momentum distributions) of the upper Dirac cone are displayed for some selected

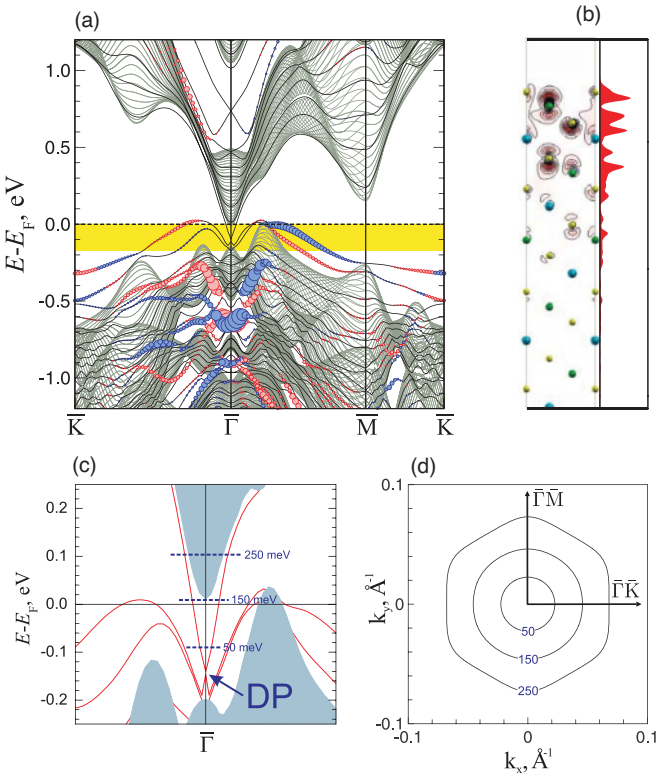

FIG. 5. (Color) (a) FLEUR-calculated band structure of a symmetric 39-layer $TlBiTe_2$ film with the Te-terminated (0001) surface. The color coding follows the one in Fig. 3. (b) The right panel shows the spatial distribution of the $\bar{\Gamma}$ Dirac-state charge density in the $(11\bar{2}0)$ plane and integrated over the (x,y) plane. (c) VASP-calculated surface electronic structure of $TlBiTe_2$ at (around) the $\bar{\Gamma}$ point with indicated cut energies shown in Fig. 5. (d) Constant energy cuts of the Dirac cone with energies indicated in (c) and given with respect to the Dirac point (DP).

energies given with respect to the Dirac point. As follows from the figure, the Dirac surface state is isotropic in the (x,y) plane. However, its shape becomes hexagonal for energies around 250 meV where it overlaps with the conduction bulk bands. This agrees well with Ref. 22, where the first deviation from the circular shape is found at 260 meV above the Dirac point.

5. *TlBiSe$_2$*

More experimental data have been recently obtained for the (0001) surface of $TlBiSe_2$.[20–23] A Dirac-type band crossing at $\bar{\Gamma}$ is observed 0.4 eV below the Fermi level[20,21,23] or 0.3 eV depending on the experiment.[22] About 200 meV above and below the crossing point, the conduction and valence bands can be seen. In the $\bar{\Gamma}\bar{M}$ direction at 0.2 Å^{-1}, a maximum of the projected bulk bands is visible, which form the top of the valence band.[21] This maximum is slightly higher than the valence-band maximum at $\bar{\Gamma}$. In contrast, in the $\bar{\Gamma}\bar{K}$ direction, only a shoulder can be seen near the zone center. Only at higher momenta is a smaller maximum observed in this direction.[22] Xu and co-workers additionally analyzed the spin character of the states forming the Dirac cone, confirming the topological character of these states. Most notably, even when the spectra

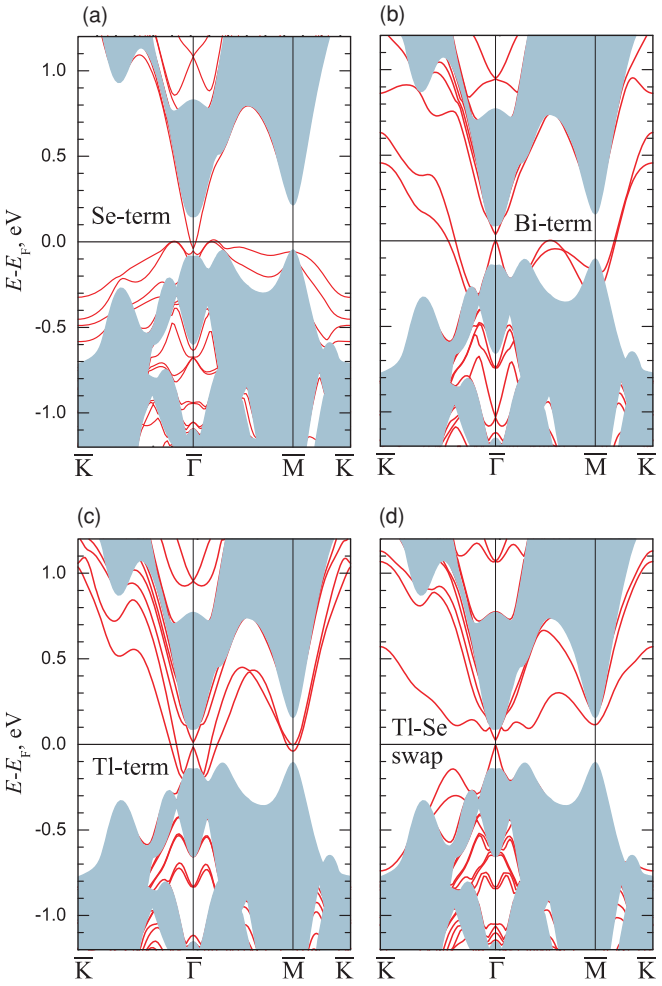

FIG. 6. (Color) Band structure of symmetric 39-layer $TlBiSe_2$ (0001) films with different surface terminations: (a) . . .-Tl-Se-Bi-Se, (b) . . .-Se-Tl-Se-Bi, (c) . . .-Se-Bi-Se-Tl, and (d) . . .-Se-Bi-Tl-Se. Red lines indicate the band structure of the films and gray areas are the projected bulk bands.

were taken in the whole momentum range between $\bar{\Gamma}$ and $\bar{K}$ or $\bar{M}$, no evidence for additional surface states was found.[21,22]

Comparison of the experimental data with our calculations (Fig. 6) shows that the bulk bands are nicely reproduced. The maxima and minima of the projected bulk regions around the $\bar{M}$ point show a gap of 300 meV, in good agreement with the experiment.[21] Also, the features of the projected bulk bands in the $\bar{\Gamma}\bar{K}$ direction are well reproduced. Comparison to calculations with different relaxations of the bulk structure show once more the importance of the structural details for the electronic structure in this family of compounds.[22] At the same time, the DP position with respect to the valence band for the Se-terminated surface [Fig. 6(a)] disagrees with the photoemission experiments. In ARPES measurements,[20–23] it lies in the middle of the gap, while in our calculation, band crossing occurs closer to the valence band, similar to the $TlBiTe_2$ case.

In Fig. 7, we show constant-energy cuts through the Dirac cone at energies between 0.09 and 0.19 eV above the Dirac point. We can analyze the spin polarization of these states for a direct comparison to the experimentally

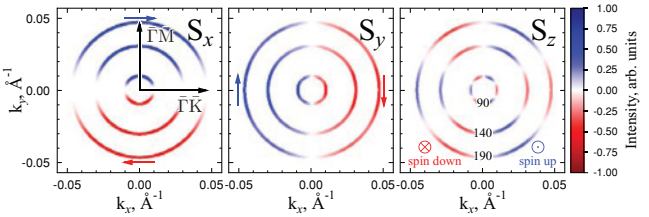

FIG. 7. (Color online) Spin polarization of the Dirac-cone states of a $TlBiSe_2$ (0001) surface with Se termination. Shown are constant energy cuts at 90, 140, and 190 meV above the Dirac point, where the spin precesses clockwise around the $\bar{\Gamma}$ point.

obtained data.[23] From these measurements, it can be seen that, above the Dirac point, the spin direction is in plane and precesses clockwise around the $\bar{\Gamma}$ point, while below that point, a counterclockwise precession is found. This is clearly confirmed by our calculations (Fig. 7). Moreover, we notice a small polarization component in the z direction, which results from the in-plane potential gradients arising from the threefold symmetry of the structure.[41] This polarization is energy dependent and is manisfested in the spin-vector deviation from the xy plane: the angle between the spin direction and the plane is equal to 21°, 39°, and 32° for the energy cuts of 90, 140, and 190 meV, respectively.

While the experimentally visible features are well reproduced, as a qualitative difference to our calculation, we notice again the presence of surface states in our band structures. Since we always considered the B-terminated surface of $TlAB_2$ compounds, all spectra show qualitatively similar surface states. Also, other calculations with B termination find a fully occupied trivial surface state coexisting with the Dirac-type states.[18,19]

Other surface terminations lead to different surface states, as is illustrated in Figs. 6(b)–6(d). Most notably, Bi- [Fig. 6(b)] and Tl- [Fig. 6(c)] terminated surfaces show partially occupied surface states that cross the Fermi level at different positions: in the Tl-terminated case, very close to the $\bar{\Gamma}$ point, and in the Bi-terminated case, they form a spin-split Fermi-surface contour encircling the $\bar{K}$ point. Thus, the occupation of the surface state follows the nominal valency of the atom at the surface. The Dirac cone at $\bar{\Gamma}$ as well as the DP are slightly affected by the surface termination.

The discrepancy between the experimental and calculated spectra can be qualitatively explained within the Tl-Se swap model [Fig. 6(d)] in which the Tl and Se atomic layers on the Tl-terminated surface are interchanged, i.e., the . . .-Se-Bi-Tl-Se surface is constructed. On this surface, most of the trivial surface states lie above E_F, close to the conduction band, while the occupied surface states lie well below the Fermi level and the DP is situated 160 meV above the valence band at $\bar{\Gamma}$ in agreement with experiment.[20–23] However, this surface is 56 meV/Å^2 less energetically favorable than the original Tl-terminated surface. Thus, in addition, this situation can not straightforwardly explain the experimentally observed absence of a trivial surface state in the spectrum. More experimental and theoretical work is necessary to resolve the problem of surface termination and structure in these compounds.

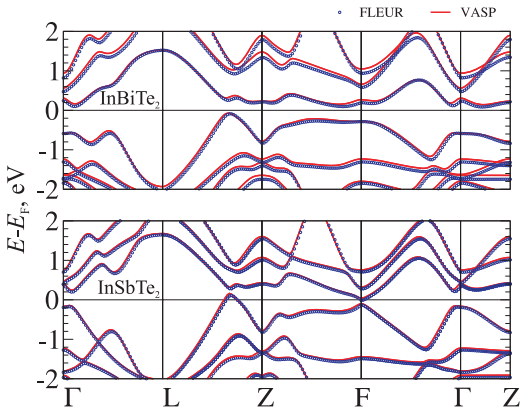

FIG. 8. (Color online) Bulk band structure of $InBiTe_2$ and $InSbTe_2$ calculated by the VASP (lines) and the FLEUR codes (circles) with spin-orbit coupling included.

6. *$InBiTe_2$ and $InSbTe_2$*

In analogy to the thallium-based compounds, we study now the crystals where indium replaces the Tl to form the $InAB_2$ compound. Experimentally, these compounds are not known and it seems that, in contrast to the (formally) monovalent Tl, the In rather acts as trivalent element: compounds such as In_2Te_3 are known to crystallize in rhombohedral forms, with one modification very similar to Bi_2Te_3.[42] In the $InATe_2$ (A = Bi, Sb) form, the optimized lattice parameters are $a = 4.565$ Å and $c = 22.388$ Å for the Bi compound, while for $InSbTe_2$ we get $a = 4.438$ Å and $c = 23.371$ Å. The internal parameter u is 0.250 and 0.244 for the Bi and Sb compounds, respectively.

From the bulk band structures (Fig. 8), we see that only $InBiTe_2$ is in the insulating state, while in $InSbTe_2$, small hole and electron pockets form along the line LZ and around the F point, respectively. In contrast to the Tl compounds, which are topological insulators, we find from an analysis of the parity of the states at the TRIMs that $InBiTe_2$ is an ordinary insulator. Comparing the band structure of $InBiTe_2$ and $InSbTe_2$, one realizes, however, that the bands at the F point are inverted with respect to each other. If $InSbTe_2$ could be deformed in a way such that a band gap opens without changing the ordering of the bands, it would get into a topologically nontrivial state.

To contrast the surface band structures of the thallides with those of the indium-based compounds, we also calculated a Te-terminated 39-layer $InBiTe_2$ film. Again, strong oscillatory interlayer relaxation of the order of 0.2 Å was found (compare Table II), but decaying more rapidly into the bulk. An inspection of the surface band structure in Fig. 9 shows a prominent surface state in the gap. This state is not connected to the valence bands along the high-symmetry lines, thus showing its topologically trivial character. A strong Rashba-type spin splitting is seen at the $\bar{\Gamma}$ point; according to symmetry, these two spin-split bands have to cross once more at the $\bar{M}$ point, where a small residual splitting indicates the interaction of the surface states at the upper and the lower surface of the film. At the center of the Brillouin zone, the surface state decays quite rapidly into the bulk; the (x, y) integrated charge density can be found at the right of Fig. 9.

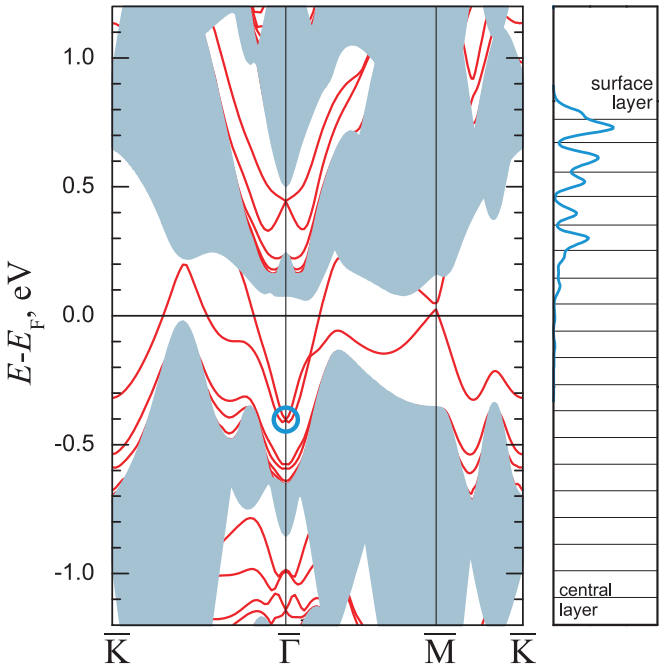

FIG. 9. (Color) Band structure of a symmetric 39-layer $InBiTe_2$ film with Te-terminated (0001) surface. The color coding follows that in Fig. 6. The right panel shows the spatial distribution of the surface-state charge density at the $\bar{\Gamma}$ point (circle) in the $(11\bar{2}0)$ plane and integrated over the (x, y) plane.

IV. SUMMARY AND CONCLUSIONS

We investigated the electronic structure of the Tl-based topological insulators $TlAB_2$ (A = Sb, Bi and B = Se, Te) by density-functional-theory calculations of the bulk and the hexagonally close-packed (0001) surfaces. We have shown that a careful treatment of the structural properties is necessary since the details of the electronic structure (and, sometimes, even its topological properties) depend sensitively on the structure of these compounds. In the surface calculations, in all cases a Dirac cone was found centered at the $\bar{\Gamma}$ point. The deep penetration of this state into the bulk made it necessary to employ rather thick films to decouple these states on the upper and lower surface. An incomplete decoupling results in a splitting of the cone, which can mask this hallmark of topological insulators in thin films.

In addition to the Dirac-cone state, other surface states that show a large Rashba-type spin splitting were found on these surfaces. Depending on the surface termination, these surface states are fully or partially occupied. While the position of the bulk states and the Dirac cone compare favorably with recent experiments on $TlBiTe_2$ (Ref. 22) and $TlSbTe_2$,[20–23] no evidence for other occupied surface states has been found experimentally. Despite this discrepancy, a good agreement between the experimentally observed spin polarization of the Dirac-type state and our calculations was found.

Finally, we contrasted these materials to isostructural $InATe_2$ compounds (A = Sb, Bi), which do not belong to the class of topological insulators. In the case of $InBiTe_2$, just the trivial surface states were found. We hope that this work inspires further research on this interesting material class, both on the theoretical and on the experimental sides, where, e.g.,

a better characterization of the surfaces and their terminations could help to resolve the last inconsistencies between our calculations and the existing ARPES measurements.

ACKNOWLEDGMENTS

We gratefully acknowledge partial support by the Department of Education of the Basque Country Government, the University of the Basque Country (Project No. GV-UPV/EHU, Grant No. IT-366-07), Ministerio de Ciencia e Inovación (Grant No. FIS2010-19609-C02-00), and the SPP 1386 Nanostrukturierte Thermoelektrika. Calculations were partly performed on SKIF-Cyberia supercomputer of Tomsk State University and Arina supercomputer of the Basque Country University. We thank S. Blügel, P. M. Echenique, A. Kimura, E. E. Krasovskii, and V. M. Kuznetsov for enjoyable discussions. We also thank I. V. Maznichenko for his assistance in preparation of some figures and important discussions.

*waptctce@sq.ehu.es

[1] L. Fu and C. L. Kane, Phys. Rev. B**76**, 045302 (2007).
[2] J. E. Moore, Nature (London) **464**, 194 (2010).
[3] M. Z. Hasan and C. L. Kane, Rev. Mod. Phys. **82**, 3045 (2010).
[4] H. Zhang, C. X. Liu, X. L. Qi, Z. Fang, and S. C. Zhang, Nat. Phys. **5**, 438 (2009).
[5] S. V. Eremeev, Yu. M. Koroteev, and E. V. Chulkov, Pis'ma Zh. Eksp. Teor. Fiz. **91**, 419 (2010) [JETP Lett. **91**, 387 (2010)].
[6] Y. Xia, D. Qian, D. Hsieh, L. Wray, A. Pal, H. Lin, A. Bansil, D. Grauer, Y. S. Hor, R. J. Cava, and M. Z. Hasan, Nat. Phys. **5**, 398 (2009).
[7] Y. L. Chen, J. G. Analytis, J. H. Chu, Z. K. Liu, S. K. Mo, X. L. Qi, H. J. Zhang, D. H. Lu, X. Dai, Z. Fang, S. C. Zhang, I. R. Fisher, Z. Hussain, and Z. X. Shen, Science **325**, 178 (2009).
[8] T. Zhang, P. Cheng, X. Chen, J. F. Jia, X. Ma, K. He, L. Wang, H. Zhang, X. Dai, Z. Fang, X. Xie, and Q. K. Xue, Phys. Rev. Lett. **103**, 266803 (2009).
[9] K. Kuroda, M. Arita, K. Miyamoto, M. Ye, J. Jiang, A. Kimura, E. E. Krasovskii, E. V. Chulkov, H. Iwasawa, T. Okuda, K. Shimada, Y. Ueda, H. Namatame, and M. Taniguchi, Phys. Rev. Lett. **105**, 076802 (2010).
[10] Y. Zhang, K. He, C. Z. Chang, C. L. Song, L. L. Wang, X. Chen, J. F. Jia, Z. Fang, X. Dai, W. Y. Shan, S. Q. Shen, Q. Niu, X. L. Qi, S. C. Zhang, X. C. Ma, and Q. K. Xue, Nat. Phys. **6**, 584 (2010).
[11] J. H. Song, H. Jin, and A. J. Freeman, Phys. Rev. Lett. **105**, 096403 (2010).
[12] W. Zhang, R. Yu, H. J. Zhang, X. Dai, and Z. Fang, New J. Phys. **12**, 065013 (2010).
[13] S. V. Eremeev, Yu. M. Koroteev, and E. V. Chulkov, Pis'ma Zh. Eksp. Teor. Fiz. **92**, 183 (2010) [JETP Lett. **92**, 161 (2010)].
[14] S. Y. Xu, L. A. Wray, Y. Xia, R. Shankar, A. Petersen, A. Fedorov, H. Lin, A. Bansil, Y. S. Hor, D. Grauer, R. J. Cava, and M. Z. Hasan, e-print arXiv:1007.5111v1.
[15] T. V. Menshchikova, S. V. Eremeev, Yu. M. Koroteev, V. M. Kuznetsov, and E. V. Chulkov, Pis'ma Zh. Eksp. Teor. Fiz. **93**, 15 (2011) [LETP Lett. **93**, 15 (2011)].
[16] H. Jin, J. H. Song, A. J. Freeman, and M. G. Kamatzidis, Phys. Rev. B **83**, 041202(R) (2011).
[17] B. Yan, C. X. Liu, H. J. Zhang, C. Y. Yam, X. L. Qi, T. Frauenheim, and S. C. Zhang, Europhys. Lett. **90**, 37002 (2010).
[18] S. V. Eremeev, Yu. M. Koroteev, and E. V. Chulkov, Pis'ma Zh. Eksp. Teor. Fiz. **91**, 664 (2010) [JETP Lett. **91**, 594 (2010)].
[19] H. Lin, R. S. Markiewicz, L. A. Wray, L. Fu, M. Z. Hasan, and A. Bansil, Phys. Rev. Lett. **105**, 036404 (2010).
[20] T. Sato, K. Segawa, H. Guo, K. Sugawara, S. Souma, T. Takahashi, and Y. Ando, Phys. Rev. Lett. **105**, 136802 (2010).
[21] K. Kuroda, M. Ye, A. Kimura, S. V. Eremeev, E. E. Krasovskii, E. V. Chulkov, Y. Ueda, K. Miyamoto, T. Okuda, K. Shimada, H. Namatame, and M. Taniguchi, Phys. Rev. Lett. **105**, 146801 (2010).
[22] Y. Chen, Z. Liu, J. G. Analytis, G. H. Chu, H. Zhang, S. K. Mo, R. G. Moore, D. Lu, I. Fisher, S. Zhang, Z. Hussain, and Z. X. Shen, e-print arXiv:1006.3843v1.
[23] S. Y. Xu, L. A. Wray, Y. Xia, R. Shankar, S. Jia, A. Fedorov, J. H. Dil, F. Meier, B. Slomski, J. Osterwalder, R. J. Cava, and M. Z. Hasan, e-print arXiv:1008.3557v1.
[24] R. A. Hein and E. M. Swiggard, Phys. Rev. Lett. **24**, 53 (1970).
[25] G. Kresse and J. Hafner, Phys. Rev. B **48**, 13115 (1993).
[26] G. Kresse and J. Furthmüller, Comput. Mater. Sci. **6**, 15 (1996).
[27] P. E. Blöchl, Phys. Rev. B **50**, 17953 (1994).
[28] G. Kresse and D. Joubert, Phys. Rev. B **59**, 1758 (1999).
[29] J. P. Perdew, K. Burke, and M. Ernzerhof, Phys. Rev. Lett. **77**, 3865 (1996).
[30] D. D. Koelling and B. N. Harmon, J. Phys. C: Solid State Phys. **10**, 3107 (1977).
[31] H. Krakauer, M. Posternak, and A. J. Freeman, Phys. Rev. B **19**, 1706 (1979).
[32] E. Wimmer, H. Krakauer, M. Weinert, and A. J. Freeman, Phys. Rev. B **24**, 864 (1981).
[33] [http://www.flapw.de].
[34] C. Li, A. J. Freeman, H. J. F. Jansen, and C. L. Fu, Phys. Rev. B **42**, 5433 (1990).
[35] K. Hoang and S. D. Mahanti, Phys. Rev. B **77**, 205107 (2008).
[36] E. F. Hockings and J. C. White, Acta Crystallogr. **14**, 328 (1961).
[37] J. Sun, J. Wang, J. Wells, Y. M. Koroteev, G. Bihlmayer, E. V. Chulkov, Ph. Hofmann, and K. Pohl, New J. Phys. **12**, 063016 (2010).
[38] Yu. M. Koroteev, G. Bihlmayer, J. E. Gayone, E. V. Chulkov, S. Blügel, P. M. Echenique, and Ph. Hofmann, Phys. Rev. Lett. **93**, 046403 (2004).
[39] J. I. Pascual, G. Bihlmayer, Yu. M. Koroteev, H.-P. Rust, G. Ceballos, M. Hansmann, K. Horn, E. V. Chulkov, S. Blügel, P. M. Echenique, and Ph. Hofmann, Phys. Rev. Lett. **93**, 196802 (2004).
[40] T. Hirahara, K. Miyamoto, I. Matsuda, T. Kadono, A. Kimura, T. Nagao, G. Bihlmayer, E. V. Chulkov, S. Qiao, K. Shimada, H. Namatame, M. Taniguchi, and S. Hasegawa, Phys. Rev. B **76**, 153305 (2007).
[41] J. Premper, M. Trautmann, J. Henk, and P. Bruno, Phys. Rev. B **76**, 073310 (2007).
[42] K. Osamura, Y. Murakami, and Y. Tomiie, J. Phys. Soc. Jpn. **21**, 1848 (1966).